

Submitted to ApJ Letters.

A *Spitzer*¹ Infrared Radius for the Transiting Extrasolar Planet HD 209458 b

L. Jeremy Richardson²

*Exoplanets and Stellar Astrophysics Laboratory, NASA's Goddard Space Flight Center,
Mail Code 667, Greenbelt, MD 20771*

`richardsonlj@milkyway.gsfc.nasa.gov`

Sara Seager

*Department of Terrestrial Magnetism, Carnegie Institution of Washington, 5241 Broad
Branch Rd NW, Washington, DC 20015*

Joseph Harrington

*Center for Radiophysics and Space Research, Cornell University, 326 Space Sciences Bldg.,
Ithaca, NY 14853-6801*

Drake Deming

*Planetary Systems Laboratory, NASA's Goddard Space Flight Center, Mail Code 693,
Greenbelt, MD 20771*

ABSTRACT

We have measured the infrared transit of the extrasolar planet HD 209458 b using the *Spitzer* Space Telescope. We observed two primary eclipse events (one partial and one complete transit) using the 24 μm array of the Multiband Imaging Photometer for *Spitzer* (MIPS). We analyzed a total of 2392 individual images (10-second integrations) of the planetary system, recorded before, during, and after transit. We perform optimal photometry on the images and use the local zodiacal light as a short-term flux reference. At this long wavelength, the transit curve has a simple box-like shape, allowing robust solutions for the stellar

²NRC Postdoctoral Research Fellow

and planetary radii independent of stellar limb darkening, which is negligible at $24\ \mu\text{m}$. We derive a stellar radius of $R_* = 1.10 \pm 0.07 R_\odot$, a planetary radius of $R_p = 1.31 \pm 0.08 R_J$, and a stellar mass of $1.135 M_\odot$. Within the errors, our results agree with the measurements at visible wavelengths. The radius of the planet therefore does not vary significantly over the factor of 40 in wavelength from the visible to $24\ \mu\text{m}$. We point out the potential for deriving extrasolar transiting planet radii to high accuracy using transit photometry at slightly shorter IR wavelengths where greater photometric precision is possible.

Subject headings: extrasolar planets, stars: individual (HD 209458)

1. Introduction

The transit of an extrasolar planet across its star allows us to measure the radius of the planet (Charbonneau et al. 2000; Henry et al. 2000; Brown et al. 2001). Of the nine known transiting planets, the prototype—HD 209458 b—has proven to have an anomalously large radius of $1.35 R_J$ (Brown et al. 2001; Wittenmyer et al. 2005). One explanation for the anomalous radius was inflation by the dissipation of tidal stress within the planet (Bodenheimer et al. 2001). However, the timing of the secondary eclipse as observed by the Spitzer Space Telescope (Deming et al. 2005), as well as improved radial velocity observations (Laughlin et al. 2005), have ruled out a non-zero orbital eccentricity of the magnitude (~ 0.03) needed by the tidal dissipation theory. Other explanations involve the fact that the observed radius is a transit radius whose value is sensitive to the opacity of the upper atmosphere (Burrows et al. 2003). The leading proposed explanation is currently the possibility of obliquity tides (Winn & Holman 2005), in which a non-zero obliquity (made possible by a spin-orbit resonance) could drive the tidal dissipation and provide the necessary energy to give the planet an inflated radius.

Our Spitzer program to measure the $24\ \mu\text{m}$ flux of HD 209458 b includes observations during transit (i.e., primary eclipse), revealing the infrared (IR) radius of the planet, which is reported in this paper. Section 2 further elaborates on why an IR radius measurement is of interest. Section 3 describes the observations; section 4 explains the photometric data analysis and radius fit. Section 5 concludes with results and discussion.

¹This work is based on observations made with the Spitzer Space Telescope, which is operated by the Jet Propulsion Laboratory, California Institute of Technology under a contract with NASA. Support for this work was provided by NASA.

2. Motivation for Infrared Radius Measurements

The reduced stellar flux at mid-IR wavelengths implies that transit photometry in this region is unable to achieve the high photometric precision obtained at visible wavelengths (Brown et al. 2001). However, stellar limb darkening weakens with increasing wavelength due to the increasing H^- free-free opacity (Vernazza et al. 1976). Thus, the fitting of transit curves to mid-IR data is simple and robust, and gives results independent of limb-darkening parameterizations. A mid-IR radius measurement is also of intrinsic interest for understanding the planet. Since the upper atmosphere is escaping (Vidal-Madjar et al. 2003), clouds and scattering layers could potentially extend to great heights. Scattering opacity due to small particles will be greatly reduced at long wavelengths, implying that the radius could be measurably smaller. A major goal of our observational program was to test this scenario by measuring the $24\ \mu\text{m}$ radius of HD 209458 b.

3. Observations

Using MIPS (Rieke et al. 2004) on the Spitzer Space Telescope (Werner et al. 2004), we observed two primary eclipse events: a half eclipse event (ingress only) on 2004 December 5 and a full eclipse event on 2005 June 27. We obtained two series of 10-second exposures using the standard MIPS raster pattern, which places the star at 14 different positions on the array. This produced 864 images during the half eclipse event and 1728 images during the full eclipse event.

4. Analysis

4.1. Photometry

We first reject obviously bad images, including those with strong ‘jailbar’ features², as well as the initial image of each cycle due to a prominent ‘first frame’ effect. This leaves 780 images for the half eclipse event, and 1612 images for the full eclipse event. We analyze each eclipse event separately. For each of the 14 raster positions, we 1) median filter the images to remove energetic particle events and hot pixels; 2) calculate the total zodiacal background from all pixels except those in a small (3×3 pixel) box surrounding the star; 3) find the center of the star to a precision of 0.05 pixel by dithering the theoretical point spread

²See the MIPS Data Handbook, available at <http://ssc.spitzer.caltech.edu/mips/dh/>

function (PSF) over the individual images and finding the best fit; 4) use the best-fit PSF to weight the pixels near the star, producing background-subtracted optimal photometry (analogous to Horne 1986) and error estimates; and 5) normalize the optimal photometry to the total background level in the frame, giving the stellar intensity relative to the zodi and thus removing any remaining instrument response variations. Once these steps are complete for each dither position, we correct the (small) baseline error introduced by normalizing to the slowly-varying zodiacal background. The Spitzer Planning of Observations Tool (SPOT) is used to estimate the magnitude of zodiacal background change (Kelsall et al. 1998). Finally, the time series at each dither position is normalized to an average of unity for the out-of-transit points.

The photometry is shown in Figure 1. The upper panel shows the aggregate data for both events combined (2392 points), and it clearly reveals the eclipse. The scatter in the points is closely consistent with the errors calculated by propagating the per-pixel errors from the Spitzer pipeline data analysis through our optimal photometry procedure. The lower panel averages the data in bins of phase width 0.001; the extreme, box-like shape of the light curve due to the lack of stellar limb darkening is quite evident. We used two independent codes to perform the optimal photometry and obtained virtually identical per-point results with both.

4.2. Light Curve Fitting

We construct a family of simple light curves by connecting intensities at the contact times with straight line segments. Three parameters uniquely describe an observed light curve (in the absence of stellar limb darkening): 1) the duration of full eclipse (i.e., the time between second and third contact, Δt_1) and 2) the duration of ingress/egress (i.e., the time between first and second contact, Δt_2), and 3) the eclipse depth. We derive best-fit values for these parameters by trial-and-error reduced chi-squared (χ_ν^2) minimization. Figure 2 shows χ_ν^2 as a function of Δt_1 and Δt_2 ; the upper panel shows the contour plot for the χ_ν^2 , and the lower panel casts the result in terms of confidence intervals. The best fit parameters (Δt_1 , Δt_2 , and eclipse depth) are listed in Table 1.

Using the analytic formulation of Seager & Mallén-Ornelas (2003), we derive the physical parameters (stellar density, planetary radius, orbital inclination) from the orbital period and the fitted parameters (Δt_1 , Δt_2 , and eclipse depth), obtained from the best-fit simple light curve. Inversion of transit curves to determine both stellar and planetary radii requires assumption of the stellar mass (Brown et al. 2001). We assumed stellar masses between 0.9 and 1.30 M_\odot (shown in Figure 3), and results for three of those assumed values are given

in Table 2, corresponding to those tabulated by Wittenmyer et al. (2005, their Figure 4). We determine realistic errors in the physical parameters by constructing 1000 synthetic light curves, based on the fitted parameters and Gaussian noise with the same per-point errors as the real data. Our quoted errors are the standard deviations of the radii and orbital inclination derived from fitting to these synthetic light curves.

Next, we check the radii and orbit inclination by removing the approximation that the light curve is comprised of straight line segments. We have developed a routine to compute light curves numerically (Richardson et al. 2006), and we include the small effect due to predicted limb darkening at $24 \mu\text{m}$, derived from a Kurucz³ model atmosphere for stellar parameters $T_e = 6000 \text{ K}$, $\log(g) = 4.5$, and $[\text{Fe}/\text{H}] = 0.0$. We validated the code by verifying that we can reproduce the fits to the very precise HST optical data from Brown et al. (2001). We adopted the derived parameters from the best-fit simple curve and calculated an exact theoretical light curve. The result is plotted as a dashed line in the lower panel of Figure 1, but it is hard to see since it is nearly identical to the simple curve. The χ^2_ν of the fits for each of the two curves to the data are nearly identical: 1.0068 for the best-fit simple curve, compared to 1.0062 for the theoretical light curve. We therefore conclude that the limb darkening is negligible at $24 \mu\text{m}$ and that the simple light curve composed of straight line segments is an accurate method of deriving the physical parameters.

Finally, we checked our results by incorporating information from the transit at visible wavelengths (Brown et al. 2001). There the transit depth is 0.0164, compared to 0.0150 ± 0.0004 at $24 \mu\text{m}$, a significant difference. The ratio of visible to IR transit depth can be used to determine the impact parameter, the minimum radius where the planet crosses the star, and thereby the orbit inclination. We used the limb darkening tabulated by a Kurucz model atmosphere (same parameters used above), and the ‘small planet’ approximation from Mandel & Agol (2002). We calculated numerically the ratio of visible to IR transit depth as a function of impact parameter. Comparing the observed ratio (1.095 ± 0.03) to this relation gives an impact parameter of 0.59 ± 0.07 , and an orbit inclination of 86.0 ± 0.6 degrees. Within the errors, this agrees with the results at visible wavelengths (Brown et al. 2001; Wittenmyer et al. 2005) and is also approximately consistent with the $i = 87.2$ value we derive internally from our IR data.

³Available from <http://kurucz.harvard.edu>. We linearly interpolate the Kurucz parameters at 20 and $40 \mu\text{m}$ to estimate the values at $24 \mu\text{m}$.

5. Results and Discussion

We have computed the stellar density directly from the observable quantities from the best-fit simple curve (Seager & Mallén-Ornelas 2003). Assuming a stellar mass allows us to calculate the stellar radius. This empirical mass-radius relation is shown in Figure 3, where we have calculated the radii for stellar masses from 0.9 to 1.3 M_{\odot} . We break the degeneracy by intersecting the stellar radius curve with the mass-radius relation from Cody & Sasselov (2002), shown as the dashed line, following Wittenmyer et al. (2005, their Figure 5). On this basis, we derive the stellar mass to be $M = 1.135 M_{\odot}$, with $R_{*} = 1.10 R_{\odot}$ and $R_p = 1.31 R_J$. Our result for the planetary radius agrees with the results at visible wavelengths: $R_p = 1.347 \pm 0.060 R_J$ (Brown et al. 2001) and $1.35 \pm 0.07 R_J$ (Wittenmyer et al. 2005). Also shown is the mass-radius relation for a zero-age main sequence star from Claret & Gimenez (1989), which intersects the empirical relation at the same point. Such exact agreement is probably fortuitous but suggests that the determination of the radii is not strongly dependent on the age of the star.

We are encouraged by the fact that the photometric precision we obtain for the IR radius of the planet is similar to the current results at visible wavelengths (Wittenmyer et al. 2005), in spite of the fact that the visible photometric observations are more than an order of magnitude more precise than our 24 μm photometry. We attribute this to the character of the IR transit curve, where the lack of limb darkening produces a simple transit shape, from which radius information can be extracted with maximum efficiency. We point out that photometry at other accessible Spitzer wavelengths such as 8 and 16 μm would provide much higher photometric precision for bright transiting systems, because the stellar flux will be much higher, and the zodiacal background will not be a limiting factor. Limb darkening remains sufficiently weak at these shorter IR wavelengths to maintain a relatively simple transit light curve shape. Considering also that Spitzer’s heliocentric orbit allows uninterrupted observations of complete transits, we suggest that IR transit photometry from Spitzer may be the optimal method for precise radius determination in bright transiting planet systems.

This work is based on observations made with the Spitzer Space Telescope, which is operated by the Jet Propulsion Laboratory, California Institute of Technology under a contract with NASA. Support for this work was provided by NASA. LJR acknowledges support as an NRC Postdoctoral Fellow at NASA Goddard.

Facilities: Spitzer(MIPS)

REFERENCES

- Bodenheimer, P., Lin, D. N. C., & Mardling, R. A. 2001, *ApJ*, 548, 466
- Brown, T. M., Charbonneau, D., Gilliland, R. L., Noyes, R. W., & Burrows, A. 2001, *ApJ*, 552, 699
- Burrows, A., Sudarsky, D., & Hubbard, W. B. 2003, *ApJ*, 594, 545
- Charbonneau, D., Brown, T. M., Gilliland, R. L., & Noyes, R. W. 2003, in *IAU Symposium*
- Charbonneau, D., Brown, T. M., Latham, D. W., & Mayor, M. 2000, *ApJ*, 529, L45
- Claret, A. & Gimenez, A. 1989, *A&AS*, 81, 37
- Cody, A. M. & Sasselov, D. D. 2002, *ApJ*, 569, 451
- Deming, D., Seager, S., Richardson, L. J., & Harrington, J. 2005, *Nature*, 434, 740
- Henry, G. W., Marcy, G. W., Butler, R. P., & Vogt, S. S. 2000, *ApJ*, 529, L41
- Horne, K. 1986, *PASP*, 98, 609
- Kelsall, T., Weiland, J. L., Franz, B. A., Reach, W. T., Arendt, R. G., Dwek, E., Freudenreich, H. T., Hauser, M. G., Moseley, S. H., Odegard, N. P., Silverberg, R. F., & Wright, E. L. 1998, *ApJ*, 508, 44
- Laughlin, G., Wolf, A., Vanmunster, T., Bodenheimer, P., Fischer, D., Marcy, G., Butler, P., & Vogt, S. 2005, *ApJ*, 621, 1072
- Mandel, K. & Agol, E. 2002, *ApJ*, 580, L171
- Richardson, L. J., Seager, S., Deming, D., Harrington, J., Barry, R. K., Rajagopal, J., & Danchi, W. C. 2006, in *IAUC 200, Direct Detection of Exoplanets: Science and Techniques*, in press, ed. C. Aime & F. Vakili
- Rieke, G. H., Young, E. T., Engelbracht, C. W., Kelly, D. M., Low, F. J., Haller, E. E., Beeman, J. W., Gordon, K. D., Stansberry, J. A., Misselt, K. A., Cadien, J., Morrison, J. E., Rivlis, G., Latter, W. B., Noriega-Crespo, A., Padgett, D. L., Stapelfeldt, K. R., Hines, D. C., Egami, E., Muzerolle, J., Alonso-Herrero, A., Blaylock, M., Dole, H., Hinz, J. L., Le Floch, E., Papovich, C., Pérez-González, P. G., Smith, P. S., Su, K. Y. L., Bennett, L., Frayer, D. T., Henderson, D., Lu, N., Masci, F., Pesenson, M., Rebull, L., Rho, J., Keene, J., Stolovy, S., Wachter, S., Wheaton, W., Werner, M. W., & Richards, P. L. 2004, *ApJS*, 154, 25

- Seager, S. & Mallén-Ornelas, G. 2003, *ApJ*, 585, 1038
- Vernazza, J. E., Avrett, E. H., & Loeser, R. 1976, *ApJS*, 30, 1
- Vidal-Madjar, A., des Etangs, A. L., Désert, J.-M., Ballester, G. E., Ferlet, R., Hébrard, G., & Mayor, M. 2003, *Nature*, 422, 143
- Werner, M. W., Roellig, T. L., Low, F. J., Rieke, G. H., Rieke, M., Hoffmann, W. F., Young, E., Houck, J. R., Brandl, B., Fazio, G. G., Hora, J. L., Gehrz, R. D., Helou, G., Soifer, B. T., Stauffer, J., Keene, J., Eisenhardt, P., Gallagher, D., Gautier, T. N., Irace, W., Lawrence, C. R., Simmons, L., Van Cleve, J. E., Jura, M., Wright, E. L., & Cruikshank, D. P. 2004, *ApJS*, 154, 1
- Winn, J. N. & Holman, M. J. 2005, *ApJ*, 628, L159
- Wittenmyer, R. A., Welsh, W. F., Orosz, J. A., Schultz, A. B., Kinzel, W., Kochte, M., Bruhweiler, F., Bennum, D., Henry, G. W., Marcy, G. W., Fischer, D. A., Butler, R. P., & Vogt, S. S. 2005, *ApJ*, 632, 1157

Table 1. Results from χ^2_ν minimization of straight-line fits. For the best fit curve, $\chi^2_\nu = 1.0068$.

| Parameter | Value | Error |
|-------------------|--------|--------|
| Depth | 0.0150 | 0.0004 |
| Δt_1 (hr) | 2.204 | 0.058 |
| Δt_2 (hr) | 0.400 | 0.051 |

Table 2. Derived physical parameters from best fit to straight-line segments, for three assumed values of the stellar mass. These parameters were derived for a range of stellar masses from 0.93 to 1.30 M_{\odot} . (See Figure 3.)

| Parameter | Value | | | Error |
|--------------------------------------|-------|-------|-------|-------|
| Assumed Stellar Mass (M_{\odot}) | 0.93 | 1.10 | 1.19 | - |
| Stellar Radius (R_{\odot}) | 1.031 | 1.090 | 1.119 | 0.066 |
| Planetary Radius (R_J) | 1.229 | 1.300 | 1.334 | 0.083 |
| Orbital Inclination (deg) | 87.24 | 87.24 | 87.24 | 0.76 |

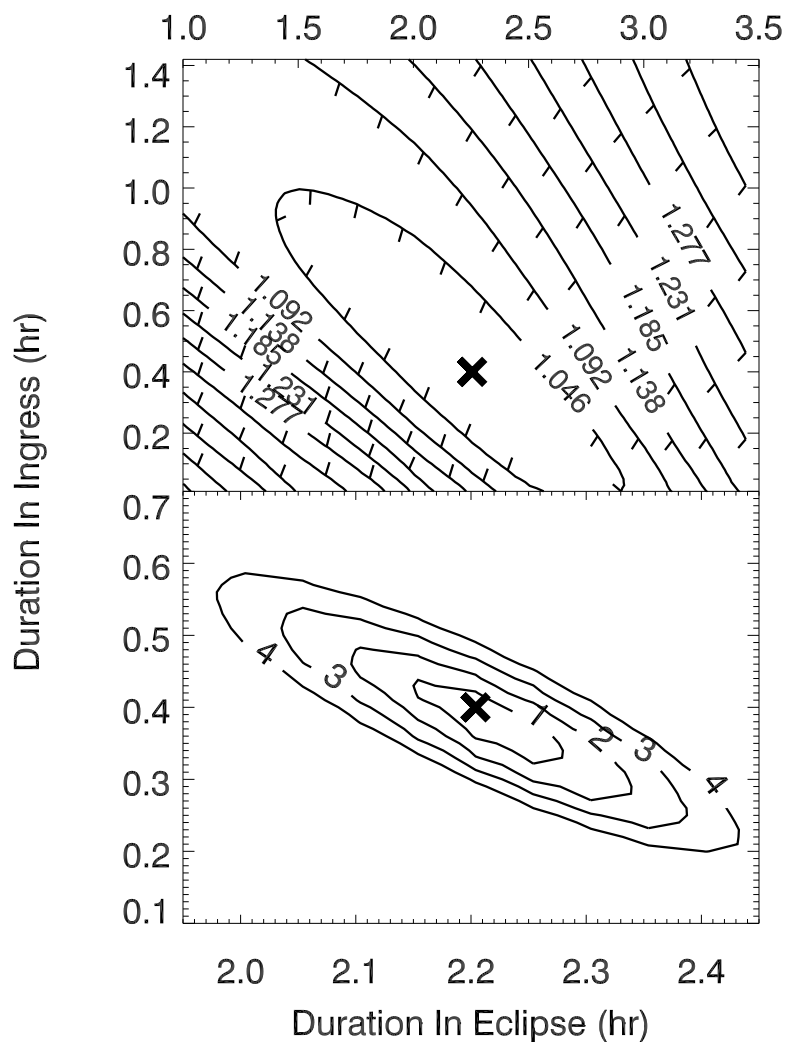


Fig. 1.— *Upper Panel:* All 2392 measurements versus heliocentric phase. *Lower Panel:* Data averaged in phase (bin size = 0.001 in phase); also shown are the best fit straight-line curve (solid line) and the exact theoretical light curve (dashed line, difficult to see), calculated using the best-fit physical parameters derived from the straight-line curve. Heliocentric phase was computed using the T_0 value from Wittenmyer et al. (2005) and the orbital period from Charbonneau et al. (2003).

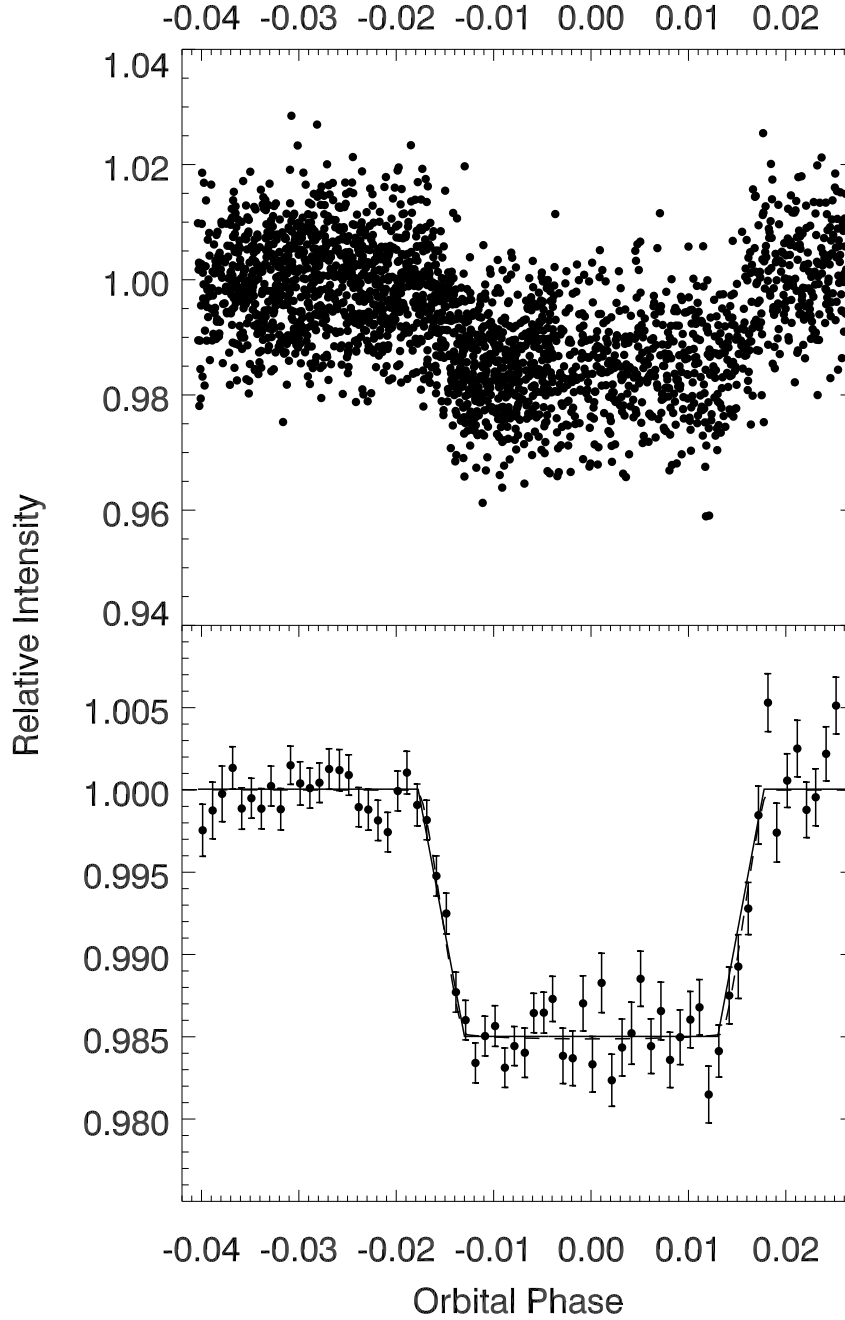


Fig. 2.— *Upper Panel:* Contour plot of reduced chi-squared fit (χ^2_ν). *Lower Panel:* Same result, but converted to confidence interval in standard deviations (note different scale). In both panels, the minimum χ^2_ν (1.0068) is marked by an X.

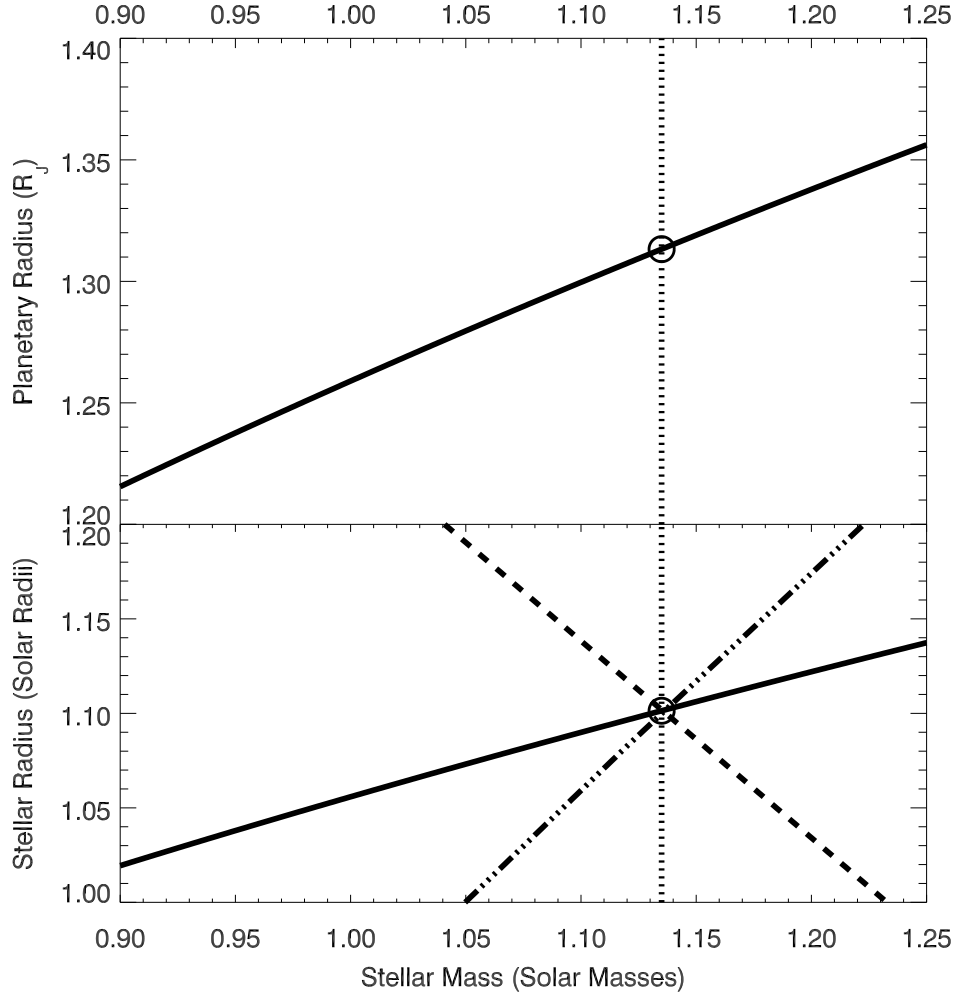


Fig. 3.— The stellar density derived from the best-fit parameters can be transformed to stellar radius by assumption of a range of stellar masses. The transit data therefore yield an empirical mass-radius relation. *Upper Panel:* Planetary radius as a function of assumed stellar mass. *Lower Panel:* Stellar radius as a function of assumed stellar mass. Dashed line represents mass-radius relation from (Cody & Sasselov 2002); dot-dash line is the mass-radius relation for a zero-age main sequence star (Claret & Gimenez 1989). Intersection of these relations with the empirical curve to the assumed stellar masses allows a determination of the stellar mass ($1.135 M_{\odot}$), marked by the vertical dotted line. This reveals the best fit stellar and planetary radii, $R_{*} = 1.10 R_{\odot}$ and $R_p = 1.31 R_J$.